FFYS7086: Signal and Image Processing

Kaj Wiik

Tuorla Observatory

Spring 2022

Based partly on 'Essential radio astronomy' from `https://www.cv.nrao.edu/~sransom/web/Ch3.html` by J. J. Condon and S. M. Ransom.

Outline

Field of view limit due to bandwidth

Bandwidth $\Delta\nu$ limits the field of view $\Delta\theta$ as follows:

$$\frac{\Delta\theta\Delta\nu}{\nu} \ll \theta_{\mathrm{s}} \tag{1}$$

where $\theta_{\mathrm{s}} \approx \lambda/b'$ is the synthesized beamwidth (or resolution) in radians and b' is the projected baseline seen from the source.
So, how we can do wide-field imaging?

Field of view limit due to bandwidth

Bandwidth $\Delta\nu$ limits the field of view $\Delta\theta$ as follows:

$$\frac{\Delta\theta\Delta\nu}{\nu} \ll \theta_{\mathrm{s}} \tag{1}$$

where $\theta_{\mathrm{s}} \approx \lambda/b'$ is the synthesized beamwidth (or resolution) in radians and b' is the projected baseline seen from the source.
So, how we can do wide-field imaging?

Split the bandwidth into narrow chunks (IF's).

Field of view limit due to finite bandwidth, example

Example:

VLA B-configuration, $b \approx 10\ \mathrm{km}$, $\lambda = 20\ \mathrm{cm}$ i.e. $\nu = 1.5\ \mathrm{GHz}$ the synthesized beamwidth is $\theta_\mathrm{s} \approx [(0.2\ \mathrm{m})/(10^4\ \mathrm{m})]\ \mathrm{rad} \approx 4\ \mathrm{arcsec}$.

We need to image an area of $\Delta\theta = 15\ \mathrm{arcmin} = 900\ \mathrm{arcsec}$ that corresponds to the single antenna primry beam, how large the bandwidth can be?

Field of view limit due to finite bandwidth, example

Example:
VLA B-configuration, $b \approx 10$ km, $\lambda = 20$ cm i.e. $\nu = 1.5$ GHz the synthesized beamwidth is $\theta_s \approx [(0.2\ \mathrm{m})/(10^4\ \mathrm{m})]\ \mathrm{rad} \approx 4\ \mathrm{arcsec}$.

We need to image an area of $\Delta\theta = 15\ \mathrm{arcmin} = 900\ \mathrm{arcsec}$ that corresponds to the single antenna primry beam, how large the bandwidth can be?

900 arcsec field of view can be obtained by using single channel bandwidth of

$$\Delta\nu \ll \frac{\nu\theta_s}{\Delta\theta} = \frac{1.5\times10^9\ \mathrm{Hz}\times 4\ \mathrm{arcsec}}{900\ \mathrm{arcsec}} \approx 7\ \mathrm{MHz}$$

Time smearing

Like finite bandwith, finite correlator integration time smears images with large fields. This is because Earth's rotation moves the source position in the frame of the interferometer.
This should be kept much smaller than the synthesized beam $\theta_{\rm s} \approx \lambda/b$. E.g. if tracking the north celestial pole, source $\Delta\theta$ away will move at an angular rate of $2\pi\Delta\theta/P$,
$P \approx 23^{\rm h}56^{\rm m}04^{\rm s} \approx 86164\ {\rm s}$.
If correlator averaging time is long compared this apparent movement, the synthesized beam will broaden tangentially. To minimize this

$$\Delta\theta\Delta t \ll \frac{\theta_{\rm s} P}{2\pi} \approx \theta_{\rm s} \times 1.37 \times 10^4\ {\rm s} \tag{2}$$

Time smearing, example

$$\Delta\theta\Delta t \ll \frac{\theta_\mathrm{s} P}{2\pi} \approx \theta_\mathrm{s} \times 1.37 \times 10^4 \ \mathrm{s} \qquad (3)$$

Example

Like in the previous example, if we want to image an area of $\Delta\theta = 900\ \mathrm{arcsec}$ when $\theta_\mathrm{s} = 4\ \mathrm{arcsec}$, the averaging time should be

$$\Delta t \ll \frac{\theta_\mathrm{s}}{\Delta\theta} \times 1.37 \times 10^4 \ \mathrm{s} = \frac{4\ \mathrm{arcsec}}{900\ \mathrm{arcsec}} \times 1.37 \times 10^4 \ \mathrm{s} \approx 60\ \mathrm{s}$$

Note that we are considering here the **correlator integration time**, i.e. the integration time of a single visibility data point. The full image integration time can be practically anything: minutes, hours and even longer if the source structure does not change.

System temperature $T_{\rm sys}$

$$\boxed{T_{\rm s} = T_{\rm cmb} + T_{\rm rsb} + \Delta T_{\rm source} + [1 - \exp(-\tau_{\rm A})]T_{\rm atm} + T_{\rm spill} + T_{\rm r} + \cdots.} \quad (3.150)$$

There are seven antenna-temperature contributions listed explicitly in Equation 3.150:

1. $T_{\rm cmb} \approx 2.73$ K is from the nearly isotropic cosmic microwave background.
2. $T_{\rm rsb}$ is the average sky brightness temperature contributed by all "background" radio sources. Extragalactic sources add [27]
$$\left(\frac{T_{\rm rsb}}{0.1 \text{ K}}\right) \approx \left(\frac{\nu}{1.4 \text{ GHz}}\right)^{-2.7} \quad (3.151)$$
in all directions, and the Galactic plane is a bright diffuse source at low ($\nu < 0.5$ GHz) frequencies [43].
3. $\Delta T_{\rm source}$ is from the astronomical source being observed, written with a Δ to emphasize that it is usually much smaller than the total system noise: $\Delta T_{\rm source} \ll T_{\rm s}$. For example, in the $\nu_{\rm RF} \approx 4.85$ GHz sky survey made with the 300-foot telescope, the system noise was $T_{\rm s} \approx 60$ K, but the faintest detected sources added only $\Delta T_{\rm source} \approx 0.01$ K.
4. $[1 - \exp(-\tau_{\rm A})]T_{\rm atm}$ is the brightness of atmospheric emission in the telescope beam (Section 2.2.3).
5. $T_{\rm spill}$ accounts for spillover radiation that the feed picks up in directions beyond the edge of the reflector, primarily from the ground.
6. $T_{\rm r}$ is the **radiometer noise temperature** attributable to noise generated by the radiometer itself, referenced to the radiometer input. All radiometers generate noise, and any radiometer can be represented by an equivalent circuit consisting of a noiseless radiometer whose input is connected to a resistor of temperature $T_{\rm r}$. Radiometer noise is usually minimized by cooling the radiometer to cryogenic temperatures. However, radiometers are not just matched resistors, so $T_{\rm r}$ may be either lower or higher than the physical temperature of the radiometer itself.
7. "..." represents any other noise sources that might be important. An example is emission resulting from ohmic losses in the long slotted waveguide feed at Arecibo (Figure 3.25).

Sensitivity I

Antenna response:

$$K = \frac{\eta_a A}{2k} 10^{-26} = \frac{A_{eff}}{2k} 10^{-26} = \frac{T_a}{S} \left[\frac{\mathrm{K}}{\mathrm{Jy}}\right] = \mathrm{DPFU} \tag{4}$$

System response **SEFD**: what amount of source flux increases the system noise as much as the noise of the receiving equipment when $T_a = 0$:

$$\mathrm{SEFD} = \frac{T_{sys}}{\mathrm{DPFU}} = \frac{2kT_{sys}}{A_{eff}} \cdot 10^{-26} \quad [\mathrm{Jy}] \tag{5}$$

Baseline sensitivity for antennas i and j (η_s = system efficiency):

$$\Delta S_{ij} = \frac{1}{\eta_s} \sqrt{\frac{\mathrm{SEFD}_i \cdot \mathrm{SEFD}_j}{2\Delta\nu\tau_{int}}} \quad [\mathrm{Jy}] \tag{6}$$

Sensitivity II

The number of baselines L is:

$$L = \frac{1}{2} \cdot N \cdot (N - 1), \tag{7}$$

where $N =$ number of antennas.

Image sensitivity I_m is standard deviation of mean of L samples (baselines),

$$\Delta I_m = \frac{1}{\eta_s} \sqrt{\frac{\mathrm{SEFD}_i \cdot \mathrm{SEFD}_j}{N(N-1)\Delta\nu\tau_{int}}} \quad [\mathrm{Jy/beam}] \tag{8}$$

Calibration and imaging

Amplitude calibration: $\rho_{ij} \Rightarrow S_{ij}$

Raw correlator constant ρ_{ij} ($\propto V_{ij}$) must be calibrated to get **correlated flux densities**:

$$S_{ij}^{c} = \rho_{ij}\, \frac{b}{\eta_s} \sqrt{\frac{\mathrm{SEFD}_i\, \mathrm{SEFD}_j}{e^{-\tau_i}\, e^{-\tau_j}}}, \qquad (9)$$

where

- ρ_{ij} = raw visibility
- b = correlator scaling factor
- η_s = system efficiency (digitization losses etc.)
- T_{sys}^{n} = system temperature at antenna n
- SEFD_n = system effective flux density at antenna n, incl. antenna gain vs. elevation and T_{sys}
- $e^{-\tau_n}$ = atmospheric absorption at antenna n

Calibration with system temperatures

Upper plot: increased T_{sys} due to rain and low elevation

Lower plot: removal of the effect.

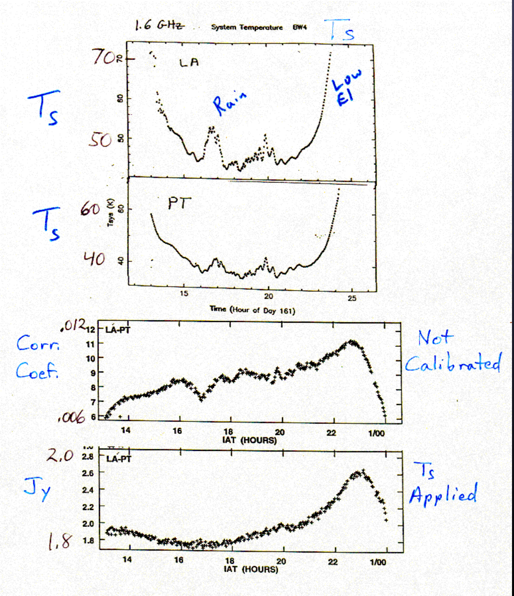

From: Ylva Pihlström, Craig Walker, Tenth Synthesis Imaging Summer School, UNM 2006.

VLBA gain curves

- Caused by gravitationally induced distortions of antenna
- Function of elevation, depends on frequency

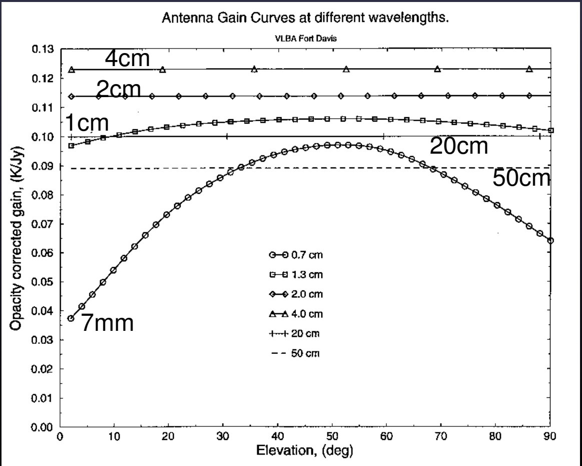

From: Ylva Pihlström, Craig Walker, Tenth Synthesis Imaging Summer School, UNM 2006.

Closure phases I

The phase of a baseline consists of three components:

$$\phi_{ij} = \phi_{ij}^{\mathrm{true}} + \phi_i^{\mathrm{err}} - \phi_j^{\mathrm{err}}, \tag{10}$$

i.e true phase due to the source structure and phase errors of individual antennas.

Closure phases I

The phase of a baseline consists of three components:

$$\phi_{ij} = \phi_{ij}^{\mathrm{true}} + \phi_i^{\mathrm{err}} - \phi_j^{\mathrm{err}}, \tag{10}$$

i.e true phase due to the source structure and phase errors of individual antennas.

If we take a sum of phases of three antennas, or a baseline triangle, we get the closure phase:

$$\begin{aligned}
\Psi_{ijk} &= \phi_{ij} + \phi_{jk} + \phi_{ki} \\
&= (\phi_{ij}^{\mathrm{true}} + \phi_i^{\mathrm{err}} - \phi_j^{\mathrm{err}}) \\
&+ (\phi_{jk}^{\mathrm{true}} + \phi_j^{\mathrm{err}} - \phi_k^{\mathrm{err}}) \\
&+ (\phi_{ki}^{\mathrm{true}} + \phi_k^{\mathrm{err}} - \phi_i^{\mathrm{err}})
\end{aligned}$$

Closure phases II

The phase-error of the second antenna is negative because visibilities are Hermitian i.e. when you swap antennas, the visibility is a complex conjugate of the original.

Closure phases II

The phase-error of the second antenna is negative because visibilities are Hermitian i.e. when you swap antennas, the visibility is a complex conjugate of the original.
Rearranging:

$$\begin{aligned}\Psi_{ijk} = {} & \phi_{ij}^{\mathrm{true}} + \phi_{jk}^{\mathrm{true}} + \phi_{ki}^{\mathrm{true}} \\ & + \phi_i^{\mathrm{err}} - \phi_i^{\mathrm{err}} \\ & + \phi_j^{\mathrm{err}} - \phi_j^{\mathrm{err}} \\ & + \phi_k^{\mathrm{err}} - \phi_k^{\mathrm{err}}.\end{aligned}$$

Closure phases II

The phase-error of the second antenna is negative because visibilities are Hermitian i.e. when you swap antennas, the visibility is a complex conjugate of the original.
Rearranging:

$$\begin{aligned}\Psi_{ijk} = \phi_{ij}^{\mathrm{true}} + \phi_{jk}^{\mathrm{true}} + \phi_{ki}^{\mathrm{true}} \\ + \phi_i^{\mathrm{err}} - \phi_i^{\mathrm{err}} \\ + \phi_j^{\mathrm{err}} - \phi_j^{\mathrm{err}} \\ + \phi_k^{\mathrm{err}} - \phi_k^{\mathrm{err}}.\end{aligned}$$

$$\Psi_{ijk} = \phi_{ij}^{\mathrm{true}} + \phi_{jk}^{\mathrm{true}} + \phi_{ki}^{\mathrm{true}} \tag{11}$$

I.e. all **antenna based** errors are cancelled. Closure phase is actually a complex quantity called the *triple product* or *bispectrum*.

SMA closure phase measurements at 682GHz

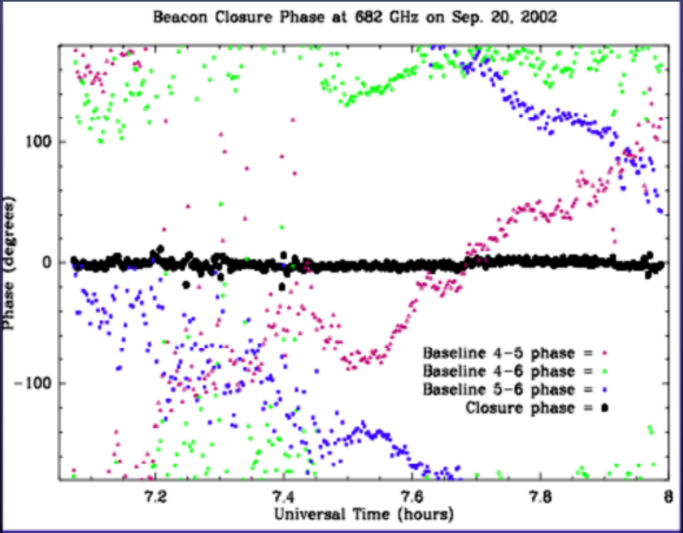

From: Rupen, Tenth Summer Synthesis Imaging Workshop, University of New Mexico, Jun 13-20, 2006

Fringe fitting and self calibration

In VLBI, the residual delays, rates ($\sim$ Doppler), and phases are in effect unknown. They are usually solved for antennas not for baselines, this is called *global fringe fitting* and gives better sensitivity (all data for a given antenna is used). In some special cases *baseline based* fringe fitting is used.

In both methods, the source is assumed to be point-like (constant phases and amplitudes), if not, a model for the source can be used.

Self calibration is solving the *antenna phases* and sometimes amplitudes (not visibility phases!!) based on a source model.

Self calibration imaging sequence

- Iterative procedure to solve for both image and gains:
  - Use best available image to solve for gains (start with point)
  - Use gains to derive improved image
  - Should converge quickly for simple sources
- Does not preserve absolute position or flux density scale

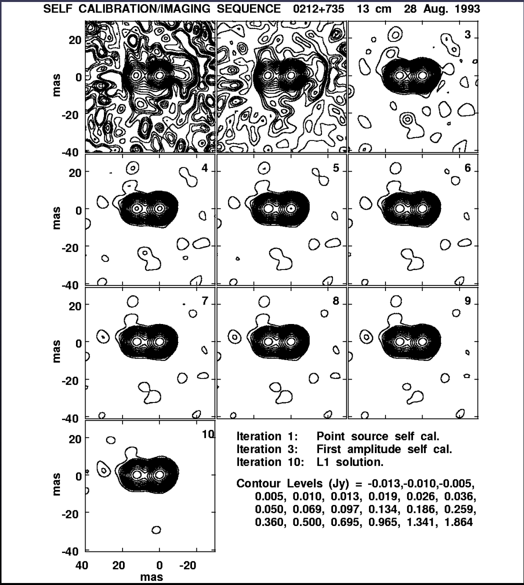

Imaging

- If the whole uv-plane would be sampled, a simple Fourier inverse transform would be enough to make images.
- Dirty image is a convolution between ideal image and the PSF (dirty beam).
- The missing information must be interpolated (and sometimes extrapolated) to avoid sidelobes/artefacts.
- Especially the 'central hole' of the uv-plane can be filled using single-dish low-resolution maps.
- Fortunately external 'known' information can be used to fill the voids, e.g.:
  - Flux is positive.
  - Sky is smooth in general.
  - Sky is a collection of rather compact emission regions.

Imaging

There are three basic methodologise to produce images from interferometry data:

- CLEAN
- Regularized Maximum Likelihood (RML) methods
  - SMILI
  - eht-imaging
- Bayesian methods
  - resolve
  - Themis & Themage
  - Comrade.jl

Themis

The Astrophysical Journal, 897:139 (38pp), 2020 July 10

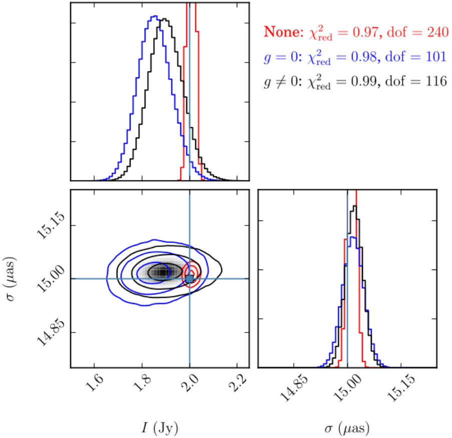

Figure 13. Posterior distribution of the size and amplitude of a symmetric Gaussian reconstructed from simulated visibility amplitude data with $\sigma_0 = 15$ μas without (red) and with (blue and black) station gain reconstruction. These include the posteriors from simulated data without gain errors (red and blue) and with significant imposed gain errors (black).

Inspecting visibility data

Before imaging it is very useful to make plots of visibility phase and amplitude:

- vs. uv-radius
- vs. time
- vs. uv-projection (slice across the uv-plane)

UV-coverage (sampling) map tells the general quality that is to be expected (sidelobe/artifact level).

These plots give first ideas what to expect from the source structure.

Sampling of the (u,v) plane

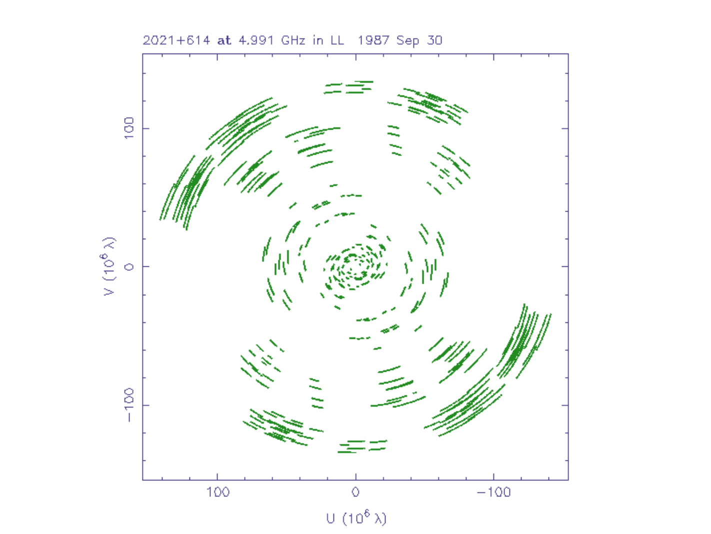

Visibility versus (u,v) radius

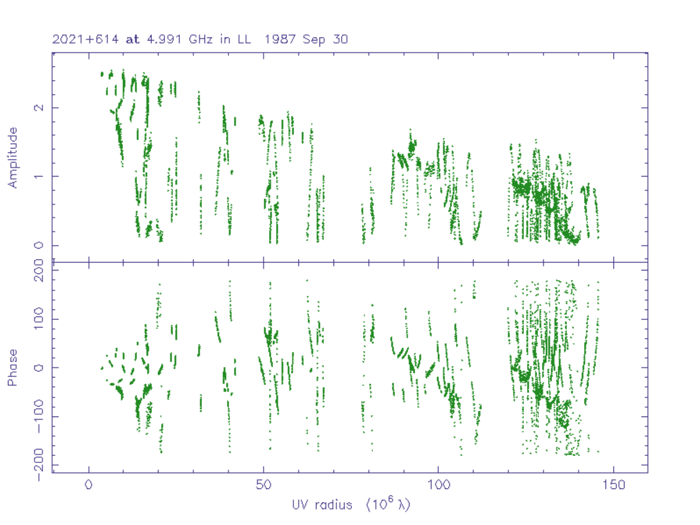

Visibility versus time

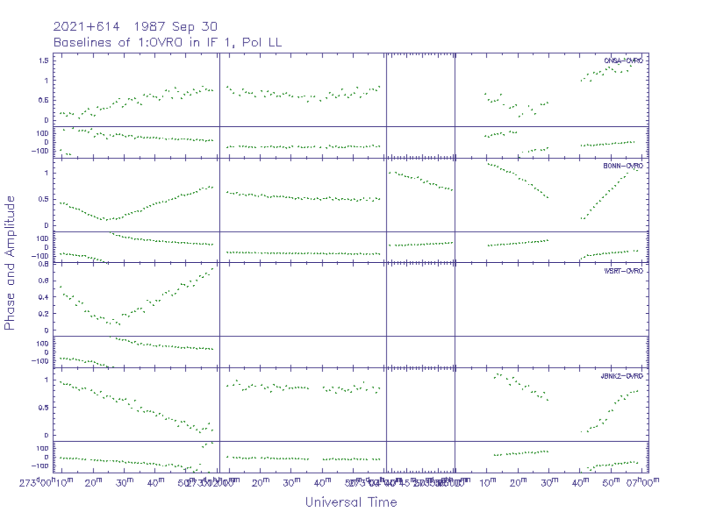

Amplitude across the (u,v) plane

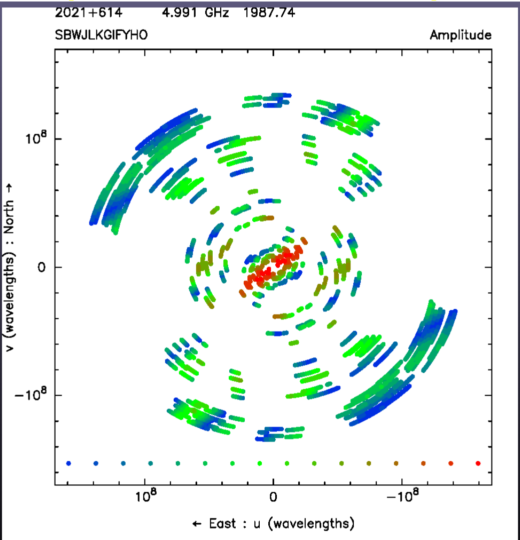

Projection in the (u,v) plane

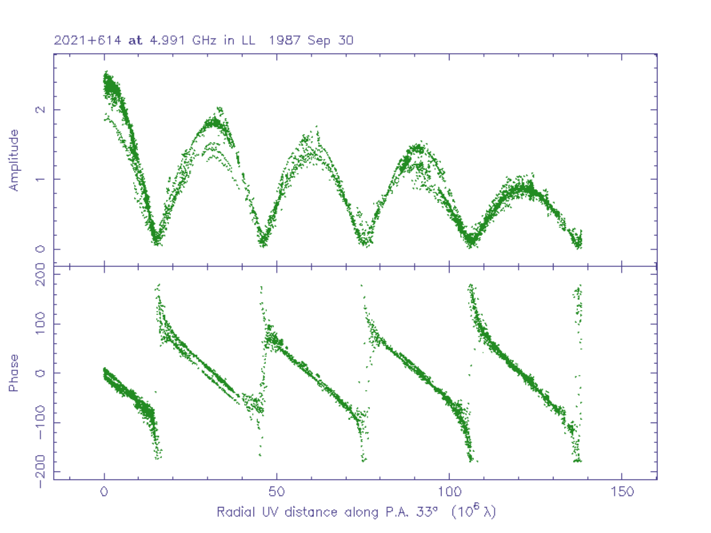

Fourier transform properties

$$F(u,v) = \mathrm{FT}\{f(x,y)\}$$

i.e.,

$$F(u,v) = \int_{-\infty}^{\infty}\int_{-\infty}^{\infty} f(x,y)\exp[2\pi i(ux+vy)]\,dx\,dy$$

Linearity

$$\mathrm{FT}\{f(x,y)+g(x,y)\} = F(u,v)+G(u,v)$$

Convolution

$$\mathrm{FT}\{f(x,y)\star g(x,y)\} = F(u,v)\cdot G(u,v)$$

Shift

$$\mathrm{FT}\{f(x-x_i,y-y_i)\} = F(u,v)\ \exp[2\pi i(ux_i+vy_i)]$$

Similarity

$$\mathrm{FT}\{f(ax,by)\} = \frac{1}{|ab|}F\left(\frac{u}{a},\frac{v}{b}\right)$$

Component profiles

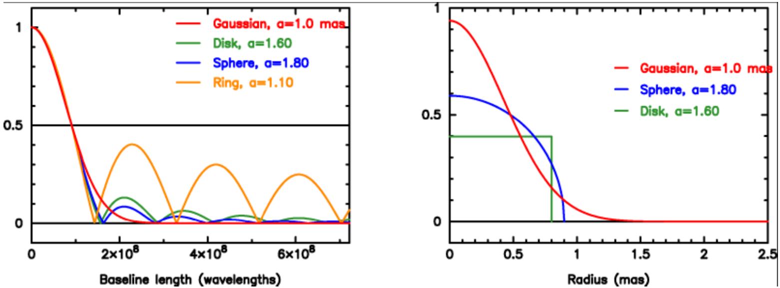

There is very little difference in the uv-plane between different source profiles down to the relative half flux level.

Simple source structures

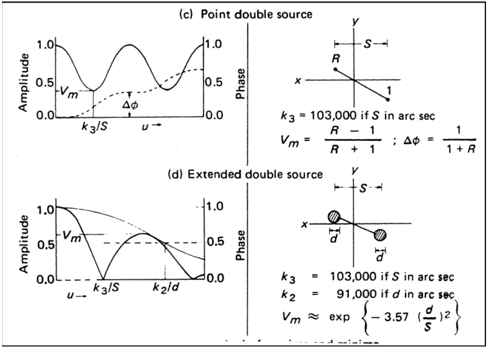

Component separation from the uv-radius (in wavelengths) of the first valley (k3/S), size of individual emission region (d [arcsec]) from the uv-radius of the half-value point of the envelope (k2/d). Amplitude is normalized.

Simple source structures, example

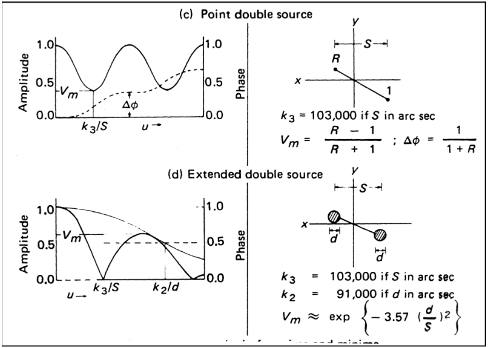

First valley at 100 M$\lambda = k_3/S$, envelope half-value point 300 M$\lambda = k_2/d$.

Double source, component separation
$S = k3/100\mathrm{M}\lambda = 103000/100e6 = 0.001\,\mathrm{arcsec} = 1\,\mathrm{marcsec}.$

Component size
$d = k2/300\mathrm{M}\lambda = 91000/300e6 = 0.0003\,\mathrm{arcsec} = 300\,\mu\mathrm{arcsec}$

Simple source structures in 2D

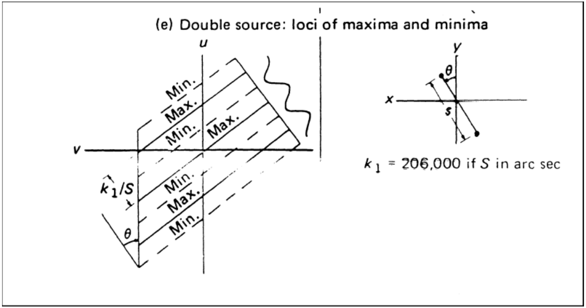

Component separation from the valley-to-valley distance (k1/S).

Source shift

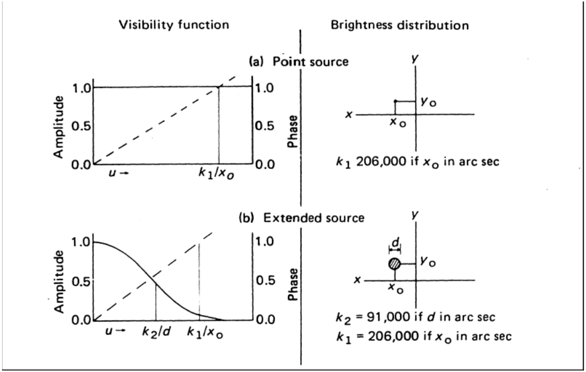

Trial model

- By inspection, we can derive a simple model:
- Two equal components, each 1.25 Jy, separated by about 6.8 milliarcsec in p.a. 33º, each about 0.8 milliarcsec in diameter (Gaussian FWHM)
- *To be refined later!*

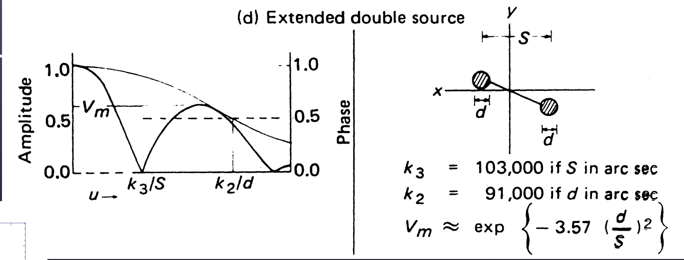

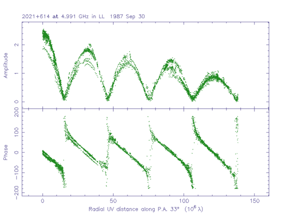

Projection in the (u,v) plane

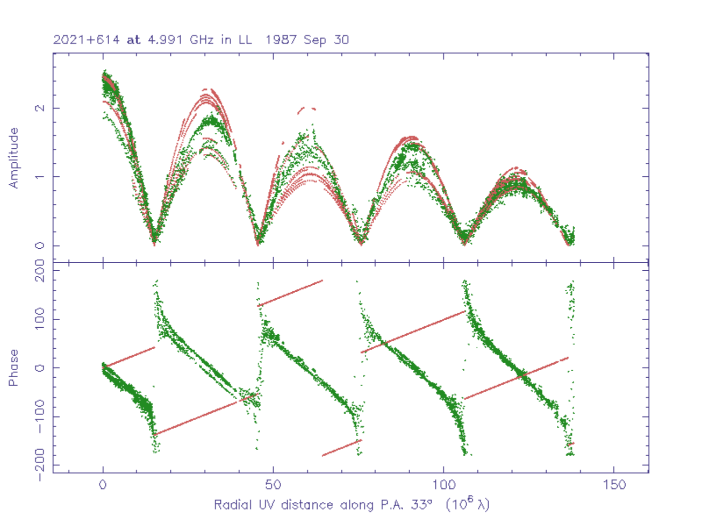

Parameters

- Example
  - Component position: (*x,y*) or polar coordinates
  - Flux density
  - Angular size (e.g., FWHM)
  - Axial ratio and orientation (position angle)
    - For a non-circular component
  - 6 parameters per component, plus a "shape"

  - This is a conventional choice: other choices of parameters may be better!
  - (Wavelets; shapelets* [Hermite functions])
    - * Chang & Refregier 2002, ApJ, 570, 447

Practical model fitting: 2021

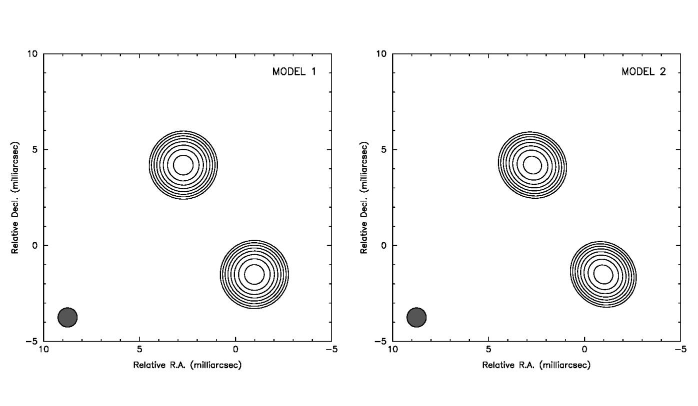

! Flux (Jy)	Radius (mas)	Theta (deg)	Major (mas)	Axial ratio	Phi (deg)	T
1.15566	4.99484	32.9118	0.867594	0.803463	54.4823	1
1.16520	1.79539	-147.037	0.825078	0.742822	45.2283	1

2021: model 2

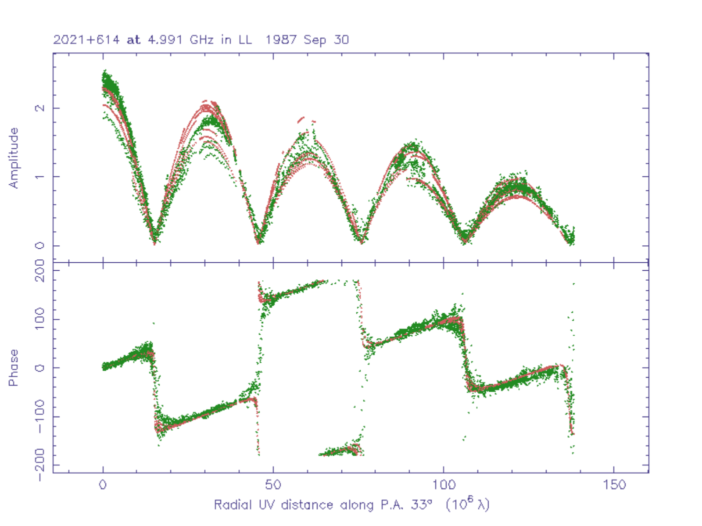
2021+614 at 4.991 GHz in LL 1987 Sep 30
Amplitude
Phase
Radial UV distance along P.A. 33° (10^6 λ)
0
1
2
200
100
0
−100
−200
0
50
100
150

Model fitting 2021

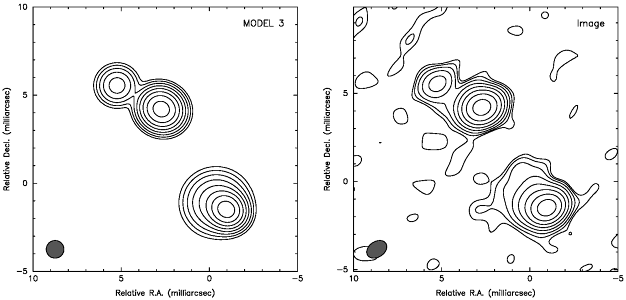

! Flux (Jy)	Radius (mas)	Theta (deg)	Major (mas)	Axial ratio	Phi (deg)	T
1.10808	5.01177	32.9772	0.871643	0.790796	60.4327	1
0.823118	1.80865	-146.615	0.589278	0.585766	53.1916	1
0.131209	7.62679	43.3576	0.741253	0.933106	-82.4635	1
0.419373	1.18399	-160.136	1.62101	0.951732	84.9951	1

2021: model 3

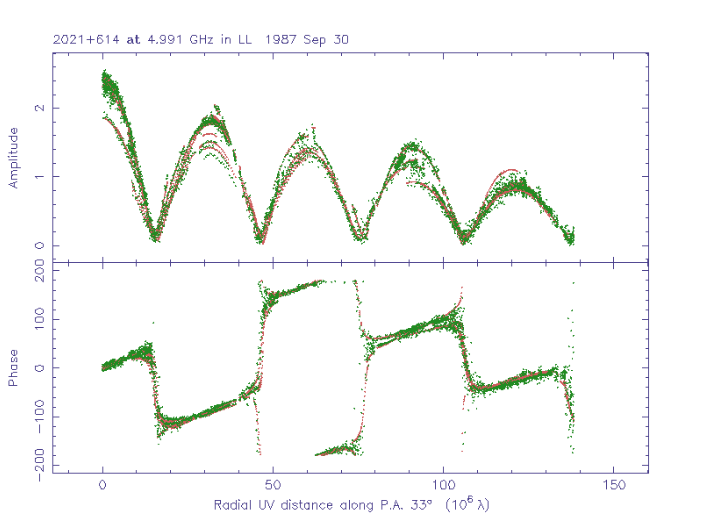
2021+614 at 4.991 GHz in LL 1987 Sep 30
Amplitude
Phase
Radial UV distance along P.A. 33° (10^6 λ)
0
1
2
200
100
0
−100
−200
0
50
100
150

Example: Space radio interferometry

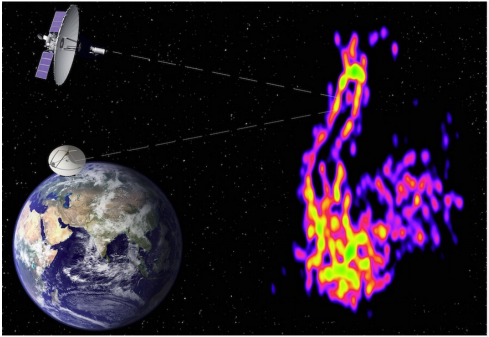

Yhdistämällä useita teleskooppeja toisiinsa pystyttiin ottamaan ennätystarkka kuva mustan aukon suihkusta. Kuva Pier Raffaele Platania INAF/IRA (kompositio); Lebedev Instituutti (RadioAstron)

03.04.2018 | Sakari Nummila

Tähtitieteilijät loivat maapalloa suuremman teleskoopin

Tuomas Savolainen käytti tähtitieteen historian tarkinta havaintolaitetta tutkiakseen mustan aukon synnyttämää plasmasuihkua. Tulokset paljastivat uutta tietoa jättiläismäisten suihkujen rakenteesta.

Example: Space radio interferometry

nature.com > nature astronomy > letters > article

MENU

nature astronomy

Altmetric: 184 More detail »

Letter

A wide and collimated radio jet in 3C84 on the scale of a few hundred gravitational radii

G. Giovannini, T. Savolainen, M. Orienti, M. Nakamura, H. Nagai, M. Kino, M. Giroletti, K. Hada, G. Bruni, Y. Y. Kovalev, J. M. Anderson, F. D'Ammando, J. Hodgson, M. Honma, T. P. Krichbaum, S.-S. Lee, R. Lico, M. M. Lisakov, A. P. Lobanov, L. Petrov, B. W. Sohn, K. V. Sokolovsky, P. A. Voitsik, J. A. Zensus & S. Tingay

Nature Astronomy **2**, 472–477 (2018)
doi:10.1038/s41550-018-0431-2
Download Citation

Received: 16 October 2017
Accepted: 27 February 2018
Published: 02 April 2018

Example: Space radio interferometry

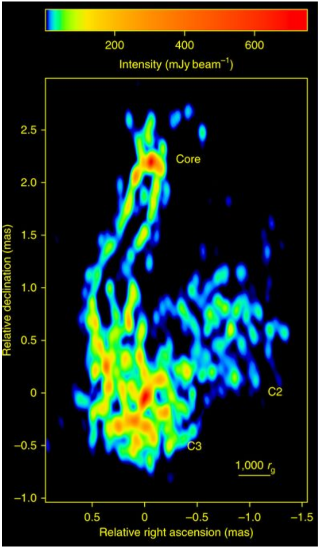

Example: Space radio interferometry

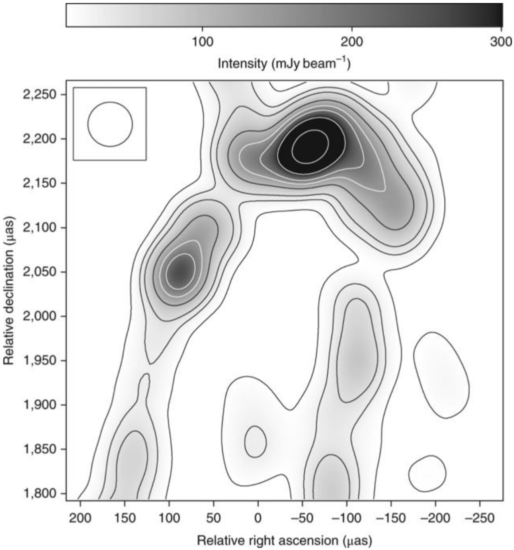

Event Horizon Telescope (EHT)

A Global Network of Radio Telescopes

EHT Newsroom: Quest for the Shadow of a Black Hole

Download Image

Astronomers Capture First Image of a Black Hole

Image Credit: EHT Collaboration

The Event Horizon Telescope (EHT) — a planet-scale array of eight ground-based radio telescopes forged through international collaboration — was designed to capture images of a black hole. Today, in coordinated press conferences across the globe, EHT researchers reveal that they have succeeded, unveiling the first direct visual evidence of a supermassive black hole and its shadow.

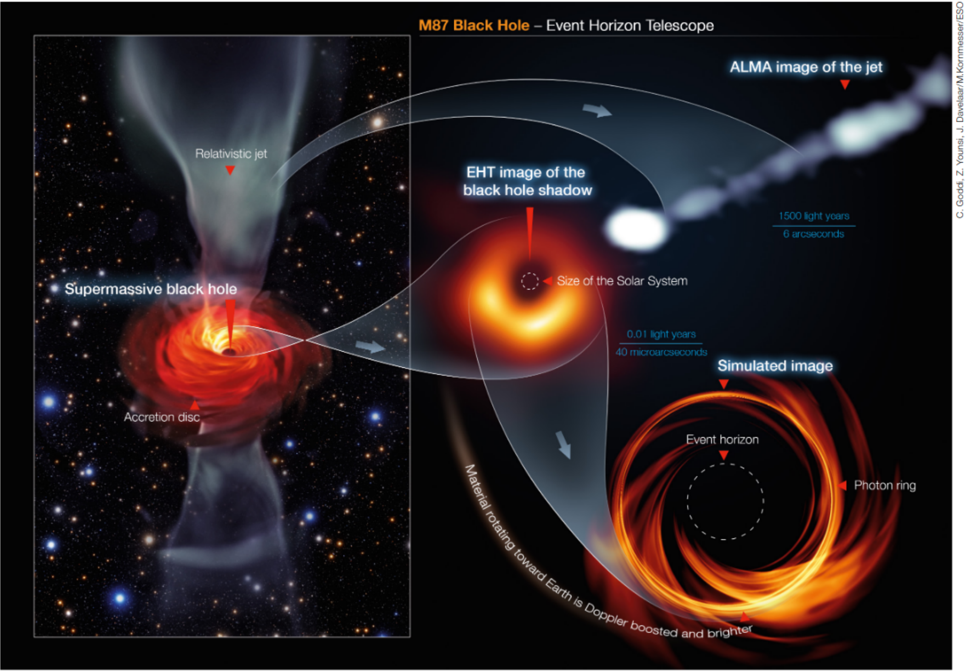
M87 Black Hole – Event Horizon Telescope
ALMA image of the jet
Relativistic jet
EHT image of the black hole shadow
1500 light years
6 arcseconds
Supermassive black hole
Size of the Solar System
0.01 light years
40 microarcseconds
Simulated image
Accretion disc
Event horizon
Photon ring
Material rotating toward Earth is Doppler boosted and brighter
C. Goddi, Z. Younsi, J. Davelaar/M.Kornmesser/ESO

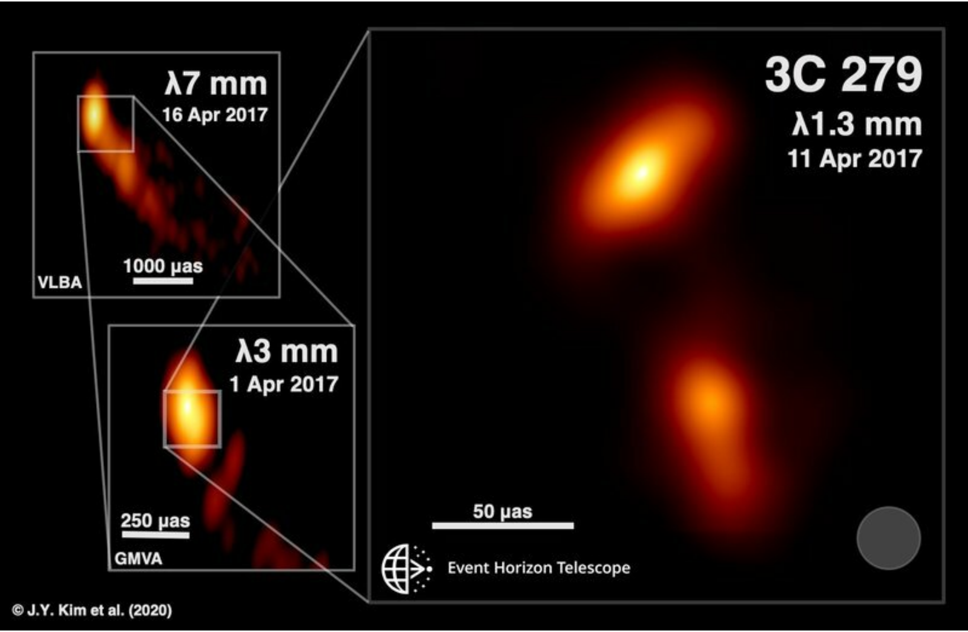
λ7 mm
16 Apr 2017
1000 µas
VLBA
λ3 mm
1 Apr 2017
250 µas
GMVA
3C 279
λ1.3 mm
11 Apr 2017
50 µas
Event Horizon Telescope
© J.Y. Kim et al. (2020)

Useful links

https://www.youtube.com/watch?v=PLPEcu6523Q

https://launchpad.net/apsynsim

Thompson, Moran & Swenson “Interferometry and Synthesis in Radio Astronomy” can be freely downloaded from https://link.springer.com/book/10.1007/978-3-319-44431-4